Adaptive Electromagnetic Damper for Frequency Selective Wrist Tremor Suppression

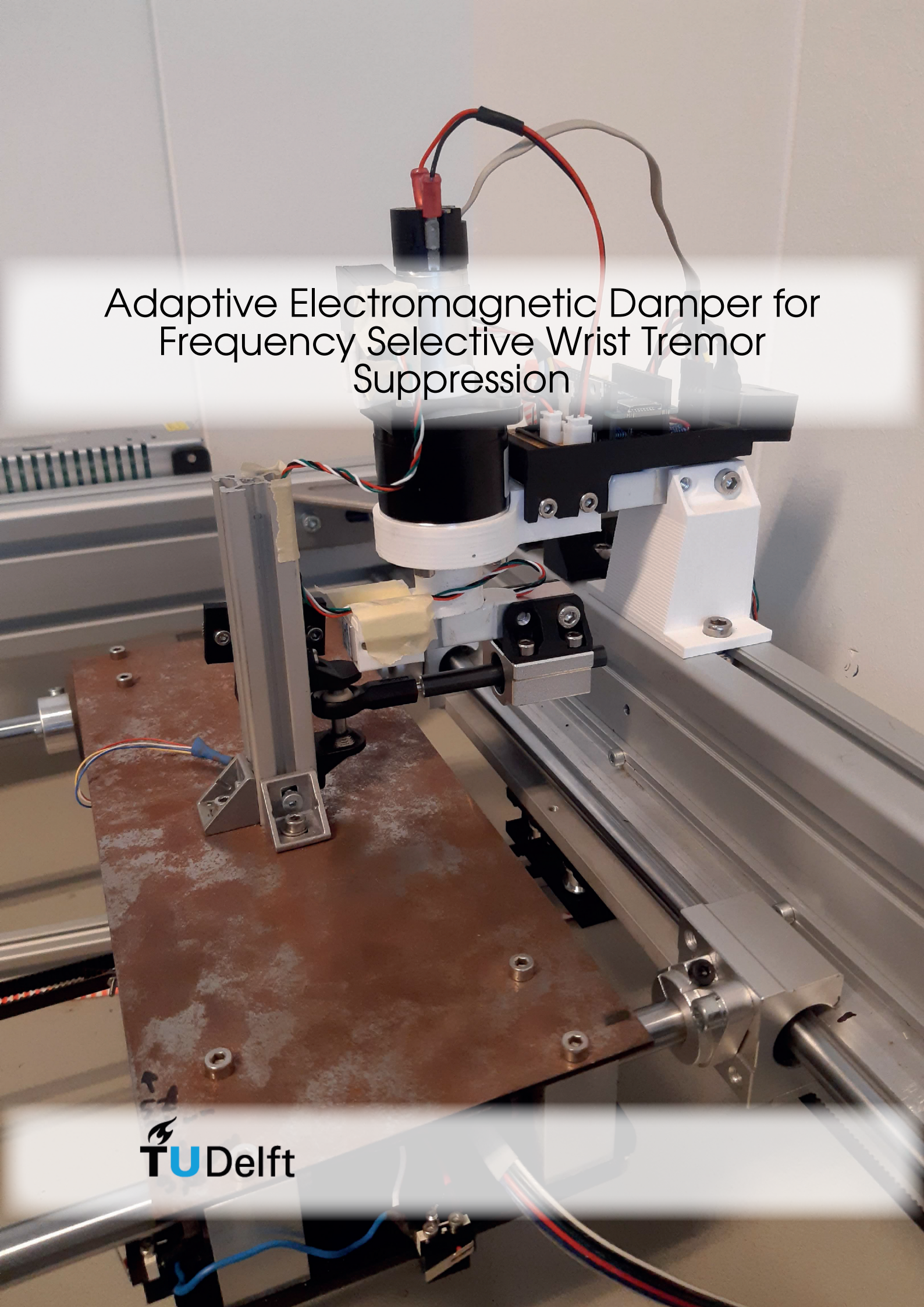

TU Delft

Preface

Despite current efforts to suppress tremor, few devices satisfy functional requirements to compete with current clinical treatments. Acknowledging this, IJsbrand De Lange founded the company STIL B.V. to further develop and work towards a functional and ergonomic tremor suppression product that uses the principle of noise-canceling to counteract forearm tremor. This product cannot directly be applied to the wrist, so a different solution is needed for wrist tremor suppression. The vision of STIL B.V. is to keep voluntary movement unrestrained whilst maintaining a high tremor reduction level. Combination of a novel wrist tremor suppression system and the forearm tremor suppression system would result in a system that restores arm functionality for tremor patients. Regained functionality of the arm enables patients to perform daily and work-related activities previously challenging, improving their quality of life.

DELFT UNIVERSITY OF TECHNOLOGY

THESIS

IN PARTIAL FULFILLMENT OF THE REQUIREMENTS FOR THE DEGREE OF MSC IN MECHANICAL ENGINEERING

Adaptive Electromagnetic Damper for Frequency Selective Wrist Tremor Suppression

Author
Hugo VAN DER KORT
4155513

Thesis Committee:
Dr. ir. W. MUGGE
Dr. ir. A. SCHOUTEN
prof. dr. ir. P. BREEDVELD
ir. IJ. DE LANGE

December 20th 2019

TU Delft

Table of Contents

Semi-Active Electromagnetic Damper for Frequency Selective Wrist Tremor Suppression

Hugo van der Kort
Delft University of Technology

December 20th 2019

Abstract

Pathological tremor is currently not adequately treated with medication; only 50% of patients respond and often treatment does not suppress tremor more than 60% at the cost of mild to severe side effects. In recent years, mechanical tremor suppression concepts have been developed, but none have thus far been implemented as replacements for current medication. This paper presents a proof of concept Adaptive Electromagnetic Damper (AEMD) for wrist tremor suppression. The AEMD was selected because of its low-energy requirement and its safe and silent operation. The concept prototype consists of a geared permanent magnet electromotor fitted with an encoder. A controller switches the motor leads in such a way that the motor can throttle the generated counter torque.

An AEMD prototype was constructed and mounted on a test setup for validation. Three validation objectives are proposed: maximum torque difference, continuous variation of torque at constant velocity and frequency specific torque generation. Results show that the prototype is able to attain a torque difference of 0.05 N m (21% of requirement). Furthermore, the results showed that the prototype was capable of varying the damping torque for the same frequency. Finally, experiments showed that the prototype was able to differentiate between frequencies, meaning that the prototype provided a damping torque to an input perturbation only when a pre-selected frequency was present. No evidence could be found for the same behavior if the setup was perturbed by multiple frequencies, including the pre-selected frequency.

Future efforts should be focussed towards finding the optimal gear ratio, motor construction, and a better model of the frequency selective aspect of the system. Component optimization is likely to increase the maximum torque difference. A working orthosis based on this concept could bring us one step closer to providing a stable life for tremor patients around the world.

1 Introduction

1.1 Pathological Tremor

Pathological Tremor is a movement disorder characterized by uncontrollable oscillation of a body part [10]. Globally about 25 million people have been diagnosed with a form of pathological tremor [1, 6, 14, 15, 19, 21, 24]. People suffering from pathological tremor struggle to perform daily tasks like eating, drinking, and writing [7]. Severity can vary, but even in less severe cases, patients are embarrassed by their tremor and experience reduced motivation to engage in social or work-related activities [7]. As a result, tremor patients experience social isolation, mental stress and an overall reduced quality of life. Suppressing the patients' tremor will improve social and economic wellbeing of tremor patients, but also their immediate community [17].

Tremor is a quasi-periodic motion with frequency and amplitude varying in time. Figure 1 shows an example of a measured elbow tremor signal, which shows the random variation in amplitude and the spread in frequency content. Literature research on wrist flexion-extension tremor reports a frequency range between 3 and 12 Hz. Measures used for tremor amplitude vary widely so no clear range can be defined, but a maximum tremor torque of 0.4 N m has been reported by Belda-lois et al. [3].

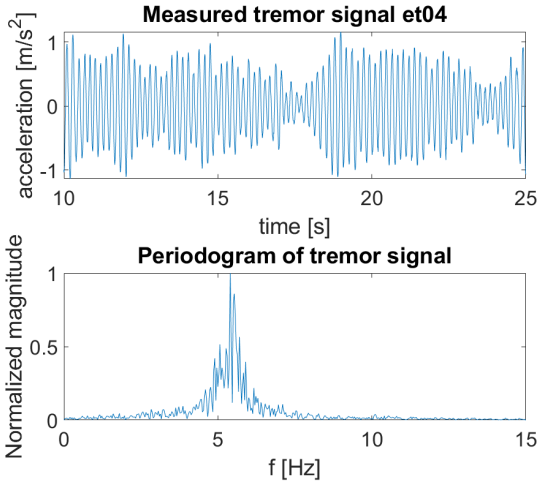

Figure 1: Plotted data of lower arm tremor measured by Timmer et al. [23]. **TOP:** A tremor signal measured as the acceleration of the lower arm showing large amplitude variations in a relatively short period of time. **BOTTOM:** A periodogram of the same data shows a spread peak indicating the presence of multiple frequencies or a time variance around a center dominant frequency.

1.2 Treatment of Tremor

Current pharmacological treatment for Essential Tremor inadequately reduces symptoms and is prone to side-effects [12]. There is no universal medication for treating every type of tremor patient. In addition, most medication is only effective for low to mild severity of Essential Tremor, introducing limited to no improvement for severe cases [10].

Besides medication, patients can turn to Functional Electrical Stimulation (FES) treatment [4] or Deep Brain Stimulation (DBS). Unfortunately, FES still suffers difficulties such as muscle fatigue and difficult electrode positioning [4, 18]. Tremor suppression effectiveness for DBS is on average $\geq$ 80%, however effectiveness tends to decrease over time [8]. Additionally DBS is invasive, costly and generally not suited for older individuals due to the health risks of surgery [7, 10]. Without a better understanding of the pathophysiology of tremorous diseases like Essential Tremor, no further improvement of current medical treatment is expected [10]. For this reason recent efforts have shifted towards mechanical tremor suppression.

Most mechanical tremor suppression research is focussed towards suppressing upper limb tremor, as tremor in these limbs causes the most impairment for patients [5, 9]. Mechanical tremor suppression can be divided into three categories.

Passive: The passive category reduces tremor amplitude by adding extra joint damping without using an external power source. Kotovsky and Rosen have proposed an orthosis based on viscous friction in 1998 [13]. This idea has been adapted with non-newtonian fluid in the Steadi-One but that device has not been clinically validated [11]. The downside of passive principles is that they suppress tremor and voluntary motion. This makes the use of a passive suppression orthosis less comfortable or tiresome.

Semi-active: Semi-active tremor suppression adds controllability to the passive suppression concepts. By continuously adjusting the amount of damping of a passive device it is possible to suppress specific frequencies. An adaptable viscous damper has been proposed by Loureiro et al. in the form of a magnetorheological(MR) damper [16]. A high level of suppression was achieved (90%), but the effect on voluntary motion was also considerable (85%). Abbasi and Afsharfard investigated the potential of piezo-material to extract tremor power and use it to counteract the tremor itself [2]. Suppression ranged between 20% and 83%, and was highly correlated with tremor frequency. Both of these concepts have not been developed into a market-ready product, but seem capable of high tremor suppression levels at low power consumption.

Active: Active tremor suppression uses actuators and sensors to exert a precise counter force to the tremor. Rocon et al. have used electromotors under the broader research project WOTAS [20], obtaining up to 80% tremor suppression. Zamanian and Richer tested an electromagnetic linear actuator on a test setup with characteristics resembling the human arm [25] and obtained 97% tremor reduction. Despite the high suppression percentages achieved by the previous two, their devices require a substantial amount of external power. The devices are also quite heavy and large making extended use uncomfortable. A more extensive overview of past efforts of mechanical tremor suppression can be found in Appendix A.1.

Unfortunately, these orthotic treatments are not yet available to provide tremor suppression in daily life activities. Tremor patients will benefit from an effective treatment, which tackles the tremor with minimal muscle strain and without uncomfortable side effects. Therefore, the goal of this research is to design a wrist tremor suppression concept and experimentally validate that it is able to reduce the amplitude of wrist tremor with minimal effect on voluntary motion.

First this research will discuss the choice of a tremor suppression concept. A Harris Profile showed the *Adaptive Electromagnetic Damper* (AEMD) to comply best with the proposed requirements. The concept was modeled and analyzed to find important component parameters and interactions. A prototype was fabricated and validated on a test setup. The validation results show that the proposed concept is able to dampen characteristic tremor frequencies, but the effect on voluntary frequencies remains for further research.

2 Concept development

2.1 Adaptive Electromagnetic Damper

For the evaluation of the concept, a prototype was designed. The characteristics of Essential Tremor were used to guide the design, as it is the most prevalent tremor pathology [15]. Furthermore, only one axis of movement was considered, because research shows that wrist ulnar-radial deviation tremor is absent in ET [22].

A Harris profile (Appendix A.2) provided a structured way of determining which principle has the most potential for a wrist tremor suppression system. From the Harris profile it is observed that active and passive categories either influence voluntary motion or require considerable external power to operate. This makes semi-active tremor suppression more appealing than passive or active concepts. With the addition of the promising results from previous semi-active suppression research a semi-active concept, Adaptive Electromagnetic Damper (AEMD), is chosen for evaluation.

A morphological chart was set up to guide the choice for concept components. First the concept's function is subdivided into subfunctions. Each subfunction has multiple possible physical implementations. By tying different implementations together a variety of concepts can be imagined. The morphological chart in Appendix **??** provided three concepts which were compared for feasibility. The chosen concept consists of a permanent magnet DC-motor, encoder, gearbox and a variable resistance. The permanent magnet DC-motor combines

the first three subfunctions into a compact structure. The gearbox makes the motor rotate at a higher velocity to increase the motor's braking potential. Tremor frequency is then determined from encoder readings. Finally the variable resistance is implemented by an electronic circuit which approximates a variable resistance using Pulse Width Modulated (PWM) switching of the motor leads. By in- and decreasing the damping at the right frequency the back-Electromotive Force (back-EMF) can be synchronized with the tremor movement, reducing influence on voluntary motion compared to that on tremor.

Using the well-understood mechanics of electromotors and adding electronic variability of the damping torque provides a less complex implementation of a variable damper compared to the concepts discussed in the previous section. Additionally, frequency-selective control of the damper torque minimizes the dampers influence on voluntary motion, while still resisting tremor frequencies.

2.2 Mathematical model

From the decision of the concept components and structure follows the construction of a prototype. However, this requires some quantified knowledge of important parameters and component interactions. A mathematical model of the concept was created to identify important parameters and their required values. Figure 2 shows an abstracted schematic of all system components and their interactions. The differential equation of the complete system was derived from the abstracted model.

Using the Euler torque balance the mechanical side of the system is described.

$$0 = \sum T - J\ddot{\theta} \tag{1}$$

$$\begin{aligned} 0 = {} & T_{voluntary} + \cancel{T_{posture}} + T_{tremor} \\ & - T_{B_{wrist}} - T_{K_{wrist}} - T_{B_{gearbox}} - NT_{B_{rotor}} \\ & - T_{emf} - \ddot{\theta} J_{hand} - \ddot{\theta} J_{gearbox} - \ddot{\theta} N^2 J_{rotor} \\ & \cancel{- F_{gravity} \cos(\theta_{wrist}) r_{hand}} \end{aligned} \tag{2}$$

$$T = T_{tremor} + T_{voluntary} \tag{3}$$

$$B = (B_{wrist} + B_{gearbox} + NB_{rotor}) \tag{4}$$

$$J = (J_{hand} + J_{gearbox} + N^2 J_{rotor}) \tag{5}$$

$$\ddot{\theta} = \frac{T - B \cdot \dot{\theta} - K_{wrist} \cdot \theta - NK_t\, i}{J} \tag{6}$$

Gravity does affect the system in certain postures of the lower arm, but it is assumed that the human is always compensating for gravity ($T_{posture}$), so it cancels from the equation.

The electric circuit is derived by using Kirchoff's voltage law.

$$\sum V = V_{emf} - V_{R_{coil}} - V_{L_{coil}} \tag{7}$$

$$0 = K_e N\dot{\theta} - R_{coil}\, i - L_{coil}\, \dot{i} \tag{8}$$

$$i = \frac{K_e N\dot{\theta} - L_{coil}\, \dot{i}}{R_{coil}} \tag{9}$$

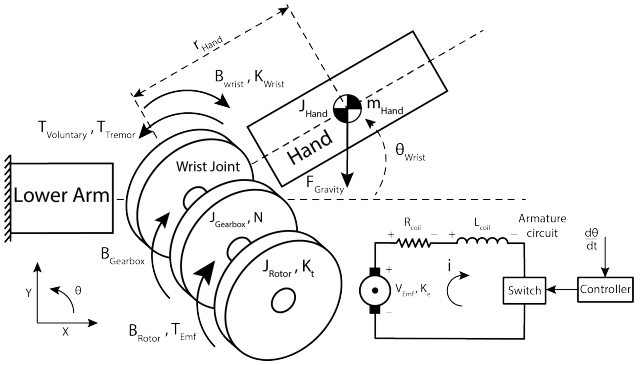

Figure 2: An abstracted representation of the Adaptive Electromagnetic Damper concept. Muscles apply a voluntary and a tremor torque ($T_{voluntary}$ and T_{tremor}) around the wrist joint. These torques are (passively) counteracted by inertia and friction in the wrist, gearbox and electromotor (J_{wrist}, $J_{gearbox}$, J_{rotor}, D_{wrist}, $D_{gearbox}$ and D_{rotor}). The wrist also has some elastic behavior captured in K_{wrist}. The gearbox has gear ratio (N) which increases the motor rotation. The back-Electromotive Force (back-EMF) of the electromotor introduces a torque (T_{emf}) opposing wrist motion. The amplitude of the back-EMF torque is dependent on the motor's torque constant K_t and electrical constant K_e. The spinning rotor creates a potential (V_{emf}) across the motor terminals, which, if short-circuited, induces an armature current (i). The coil impedance (R_{coil} and L_{coil}) primarily determine the magnitude of the armature current. The switch opens or closes the circuit and is assumed to be ideal and thus has either no impedance or infinite impedance. The controller determines whether the switch is open or closed.

Coil inductance (L_{coil}) is generally in the order of 1×10^{-4} H and $\dot{i}$ stays well below 1000 A s^{-1} for the frequencies involved, so the influence of $L_{coil}\, \dot{i}$ is neglected. Furthermore, the value for K_e is equivalent in units to K_t, which means both constants have the same value. K_t is used in the rest of the paper for both K_t and K_e. The total uncontrolled system differential equation is obtained by combining Equations 6 and 9:

$$T = J\,\ddot{\theta} + \left(B + \frac{K_t^2 N^2}{R_{coil}}\right)\dot{\theta} + K_{wrist}\,\theta \tag{10}$$

This differential equation provides a substantiated way of choosing prototype components. The motor's torque constant (K_t) and the gear ratio (N) have equal effects on the velocity-dependent damping. However, the gear ratio also influences the inertial torque as seen from Equation 6. The best way of only increasing the velocity-dependent damping is to increase the motor's $\frac{K_t^2}{R_{coil}}$ ratio. The relation between K_t and the motor's geometry and weight is quite complex so optimizing this for wrist wearability would require more time than was available for this research.

The total system is now described by a single second-order differential equation, but it assumes a short circuit of the motor terminals. The short circuit results

in a fixed velocity-damping-torque relationship, which lacks the ability to distinguish damping torque between tremor and voluntary motion. With active control over the terminal state, the system is able to make such a differentiation. Equations 11, 12 and 13 show a mathematically simplified version of controller implementation.

The control input (u) determines the magnitude of an added resistance (R_{switch}) in series with the motor coils. A higher series resistance lowers the circuit current, consequently driving down the generated back-EMF. As back-EMF is always oriented opposite to the driving torque on an electromotor, a proportional controller (gain P) is sufficient to determine the damping level. If motor velocity ($\dot{\theta}$) is filtered such that only the tremor frequency remains ($\dot{\theta}_{tremor}$), then frequency-selective damping is obtained. As such, the AEMD is able to create a damping torque that is dependent on tremor frequency.

$$u = max(0,\ min(1,\ P \cdot ||\ \dot{\theta}_{tremor}\ ||)) \tag{11}$$

$$i = \frac{K_t N \dot{\theta}_{tremor}}{R_{coil} + R_{switch}\, u} \tag{12}$$

$$T = J\,\ddot{\theta} + B\,\dot{\theta} + \frac{K_t^2 N^2}{R_{coil} + R_{switch}\, u}\dot{\theta}_{tremor} + K_{wrist}\,\theta \tag{13}$$

Equation 13 shows which parameters are critical to the maximum damping force level. However an optimization of physical components would also require a relational model between all parameters. It is for instance currently not known how a change in K_t will affect the mass and weight of the electromotor or other parameters. Therefore, both the requirements for the required force, but also practicality played a role in the selection of prototype components.

3 | Validation experiments

3.1 Prototype Requirements

To compete with the 60% tremor amplitude reduction of current medical treatment it is assumed that a damping torque of at least 0.24 N m (60% of maximum [3]) is required for a competitive alternative. Besides this, the influence on voluntary motion should be lower than that of current research. For this a new measure is defined: the selectivity ratio (SR), defined as $(\%\ \text{tremor suppression} - \%\text{voluntary motion suppression})$. For the proof-of-concept the selectivity ratio should be lower than the 13% calculated for Loureiro's MR-damper. Finally, full range of motion must be preserved, so the system must not contain any singularities where it can get stuck or show excessive angle-dependent behavior.

3.2 Prototype components

For the proof of concept a prototype AEMD is constructed. The prototype is then tested in a controlled environment, in which predetermined perturbations can be applied. The components of the prototype are indicated in Figure 3 and listed below.

Electromotor: A permanent magnet DC motor (Faulhaber 2237 24V CXR Series) is chosen. Permanent magnet motors do not have to energize stator coils, which makes it possible to create back-EMF from a rotating rotor without external power. This specific motor is small and lightweight and has an encoder built-in.

Encoder: The DC electromotor is factory fitted with a 32 pulses per revolution incremental encoder. An incremental encoder is sufficient, because the concept only requires velocity information. The encoder signals are decoded using interrupt routines, so no pulses are missed and velocity can be calculated at any desired time interval. The velocity data calculated from the encoder position is filtered and then fed to the controller.

Gearbox: An off the shelf 1:10 gearbox was chosen to keep the inertial forces limited, while still getting the motor to spin at a higher speed. Getting a custom gearbox made would not have been cost-effective and efforts to build a small and light gearbox in-house were unsuccessful.

Force sensor and amplifier: The force sensor is a TAL220 loadcell capable of measuring positive and negative forces on one axis. The load cell is combined with a HX711 loadcell amplifier breakout(Sparkfun) capable of a sample frequency of 80 Hz.

Microcontroller: An Arduino MKR Zero with a 32-bit processor was chosen based on the expected computational load of running the data acquisition and switch control. The MKR Zero runs all the sensor data acquisition and serial interfacing as well as the velocity filter, controller and input to the switching circuit. The main program runs at a loop frequency of 62.5 Hz, because it is the closest frequency to 80 Hz with an integer number of microseconds per time step. The highest frequency involved in wrist tremor is 12 Hz, so the sample frequency satisfies the Nyquist criterion. All (sensor) data is transferred to a laptop via serial connection.

Current sensor: An INA219 (Adafruit) current sensor breakout is used to monitor motor coil current. This sensor is mainly used for validation of the switching circuitry and is not essential for prototype function.

The DC-motor terminals are connected to two transistors and the current sensor such that a current only flows if both transistors are closed. Two transistors (1) seen in Figure 4, are switched using a Pulse Width Modulated (PWM) signal coming from the microcontroller. The controller input is not directly switching the transitors because of a logic voltage difference. Instead the control input switches the 5V supply of the microcontroller, which then drives the transistors. The microcontroller determines the required duty-cycle based on the velocity and

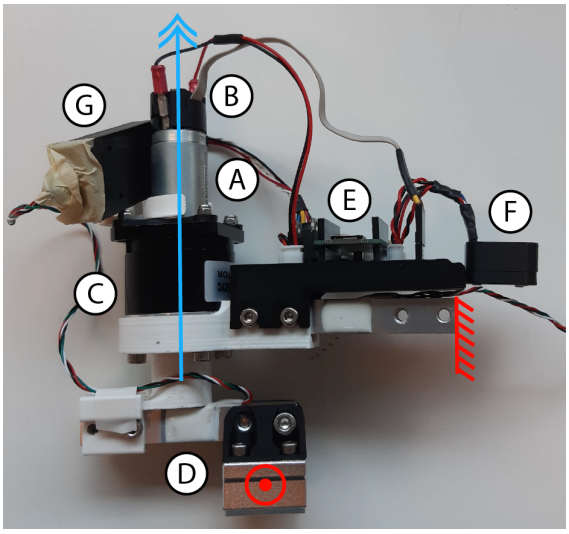

Figure 3: The AEMD prototype consisting of: a DC-motor (Faulhaber 2237 24V CXR) (*A*) with, an integrated incremental encoder (*B*), connected via a 1:10 Gearbox (*C*) to a TAL220 Loadcell (*D*) which measures the torque around the motor axle. A transistor placed between the motor leads is controlled by a MKR Zero microcontroller (*E*) and current over the motor leads is measured by an INA219 current sensor (*F*). Force sensor voltage is amplified by a HX711 amplifier (*G*). The red circle indicates where the input perturbation is applied to the prototype and the red comb shows where the prototype is fixed to the world. The blue double arrow shows the motor axis around which the force sensor measures the torque.

a proportional controller gain. The duty-cycle has a resolution of 12 bits, so the range 0-100% is divided into 4096 steps. It is also possible to set a specific duty-cycle from the laptop that is connected to the micro-controller and ignore the controller output value. For the experiments four operating modes are used:

1. MAX-MODE: The controller has no effect on the duty-cycle. The duty-cycle is manually set to 100%, which means the switches are kept closed such that maximum damping is maintained.

2. MIN-MODE: The controller has no effect on the duty-cycle. The duty-cycle is manually set to 0%, keeping the switches open, such that minimum damping is obtained.

3. CONTROL-MODE: The controller output determines the duty-cycle, switching in such a way that the highest damping occurs at a set frequency.

4. MANUAL-MODE: A user-specified value between 0% and 100% is sent to the microcontroller overwriting other modes. This allows the user to test output torque for a specific PWM duty-cycle.

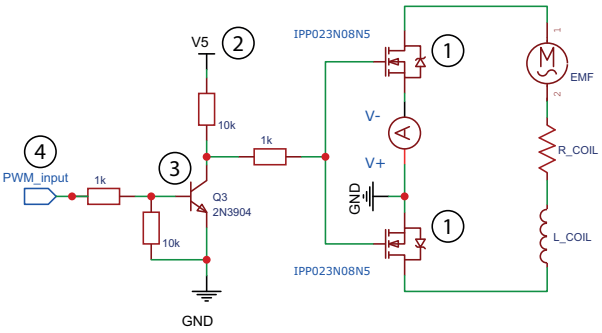

Figure 4: Electrical diagram of the switching system. Two transistors (*1*) are activated by a switched 5 Volt source (*2*) using a third transistor (*3*). The third transistor is switched by a PWM signal from the microcontroller (*4*).

3.3 Test setup

The used test setup consists of a platform which translates in one direction illustrated by Figure 5. The platform connects to a rod that telescopes to allow for a constant point of rotation. The platform is actuated by two brushless DC-motors (BLDC) via an H-bot belt and pulley transmission. The motors are driven by a dedicated BLDC motor controller board (Odrive). The wrist suppression concept is only designed for one rotation axis, so it suffices to let the platform move in one direction and to lock the other. Figure 6 shows the block scheme of the AEMD applied to the test setup.

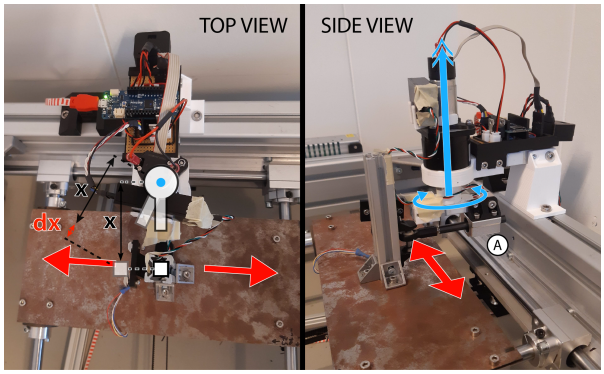

Figure 5: The test setup provides the input to the prototype by linearly oscillating in one direction (red arrows). To ensure a constant axis of rotation (blue arrows) and correct measurements from the force sensor a rod slides through a linear bearing (*A*).

The board gets its input from a dedicated PC with an interfacing program (Python). The test setup requires a user-specified array of motor setpoints as input. The array of setpoints is then played-back in one of two modes:

- *Position control:* In this mode the platform position is PID controlled. The platform moves to the position specified by the motor setpoints. This means that the prototype will not reduce the amplitude of the platform oscillation, but the force sensor registers differences in damping torque amplitude.

- *Virtual spring control:* In this mode the platform position is regulated by a loosely tuned P-controller. The platform moves as if it is dragged along by a spring attached to the setpoints. In this mode it is possible to see a reduction in platform amplitude due to prototype damping, because the actuator force ($F_{actuaotr}$) will not equalize with the damping torque ($T_{damping}$) to reduce the steady-state error.

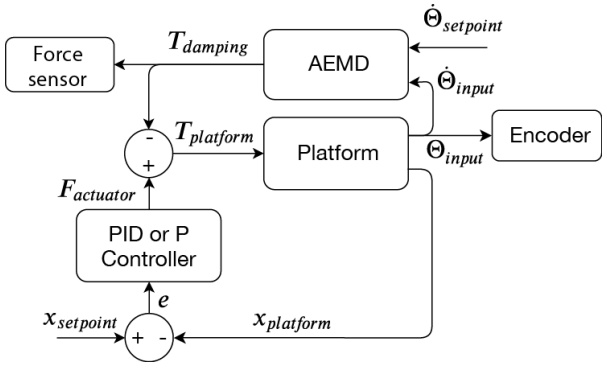

Figure 6: With the PID-controlled experiment the platform provides a position input to the prototype. The controller increases $F_{actuator}$ such that error e becomes zero. In this case, the platform position does not give any information about the prototype damping, so the force sensor between the platform and the prototype captures $T_{damping}$, the resistive torque of the motor on the platform.
In the P-controlled experiment the platform provides a force input to the prototype. $F_{actuator}$ is proportional to the distance from setpoint $x_{setpoint}$. This means that $F_{actuator}$ can be less than is required to reduce e to zero, resulting in less platform acceleration and thus a reduction in platform travel. The platform position can then be inferred from the motor encoder readings, directly showing the effect of the damper.

3.4 Validation objectives

The AEMD prototype presented in the previous section is validated using a multi-functional perturbation setup. The validation consists of three objectives:

1. Validate that the prototype is capable of generating a damping torque difference of 0.24 N m between the Max- and Min-mode.
2. Verify that the prototype can vary the damping torque between the Min- and Max-mode arbitrarily.
3. Validate that the prototype obtains a Selectivity Ratio higher than 13% for tremor frequencies ($\geq$ 3 Hz) compared to voluntary movement frequencies ($<$ 3 Hz) using frequency selective-mode.

3.5 Experiment procedure

For each experiment, input data was generated with MATLAB 20179b and transferred to the test setup PC. Each experiment followed the same general procedure:

1. Test setup platform and prototype were configured such that they were in the middle of their travel.
2. Test parameters were configured.
3. The force sensor was calibrated to within $\pm$0.01 N.
4. The trial and data acquisition were started.

An experiment consisted of several trials for which conditions were varied one by one. Each trial lasted 60 seconds and data was gathered through serial connection between the prototype and a laptop. Via an application on the laptop (SerialPlot) the sensor data was written to a .CSV-file and later loaded for post-processing (MATLAB 2019b). The following experiments were performed to find an answer for the three validation objectives:

1. The first experiment was focussed on showing the ability of the prototype to provide a counter torque to an input oscillation. Trials for multiple amplitude-frequency sinusoidal inputs were used to compare the prototype damping torque in Max-mode and Min-mode. This shows the range of torques the prototype is able to produce.
   The frequency ranged from 3 to 8 Hz and the amplitude from 5 to 25 deg prototype arm rotation. The test setup was used in position-control mode, because only the force was of interest.
2. The second experiment aimed to show the closed-loop effects of the prototype, by using the Virtual Spring-mode of the test setup. An input frequency of 3 Hz and an amplitude of 26 degrees was used. The controller output was manually changed via serial connection during the experiment.
3. The third experiment gave insight into the variability of the force between the minimum and maximum for a selected amplitude and frequency input signal. Initial results from experiment 1 showed that a frequency of 4 Hz and an amplitude of 25 degrees had the biggest force difference, which had the best potential for showing the variability. Using the Manual-mode a specific duty-cycle was set for each trial.
4. The fourth experiment focussed on the distinction of torque amplitude between frequencies. The prototype was used in Control-mode, with the selected frequency dependent on the trial condition. The input amplitude for all trials was 15 deg and between trials the input frequency was varied from 3 to 8 Hz. These trials were then done for three conditions:
   - In the first condition the trials were run with the prototype set to 5 Hz independent of the input frequency.
   - For the second condition the prototype was set to the input frequency.
   - The third condition was used as a baseline and the prototype was put into Min-mode.

3.6 Validation Measures

The data gathered from the experiments has been processed for comparison and validation against the requirements. Due to the oscillatory nature of the experiments measures are devised that capture the information of the trials in a more compact and informative way.

Mean peak torque difference Determined by subtracting the average peak torque for the Min-mode from that of the compared Torque data. The resulting value gives a measure of how much the electromagnetic effect adds to the damping torque on top of other passive sources such as inertia or friction.

Power spectral density of torque Gives a measure of torque density as a function of frequency by calculating the Welch-averaged power spectral density (PSD) of the torque measured in a trial.

4 Results

4.1 Damping torque generation

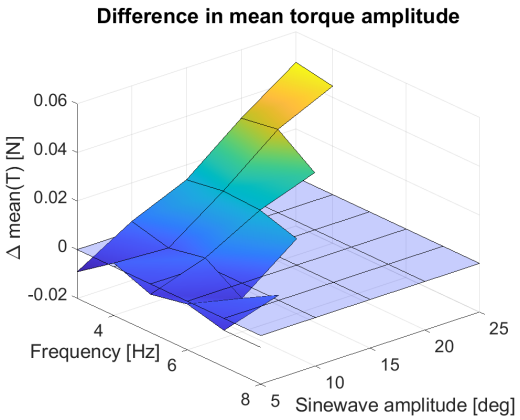

Figure 7: 3D surface plot of the tested input perturbation amplitude-frequency combinations of experiment one. Due to test setup limitations some high amplitude & frequency combinations could not be tested. The Z-axis shows the mean torque difference between the Min- and Max-mode.

Figure 7 shows the 3D surface for the *mean peak torque difference* at the tested frequency-amplitude combinations. Torque difference distributions between Min- and Max-mode are significant according to a Bonferroni-corrected threshold ($p < 0.025$) for all frequency-amplitude combinations. Figure 8 shows the absolute torque values for both Min- and Max-mode damping for the 4 Hz input. The maximum torque is 0.124 N m, which is half the required torque and only a third is due to the electrodynamic breaking.

Figure 9 shows the results from the second experiment. It shows a 50% decrease in motor amplitude when the Control input is switched from Min- to Max-value.

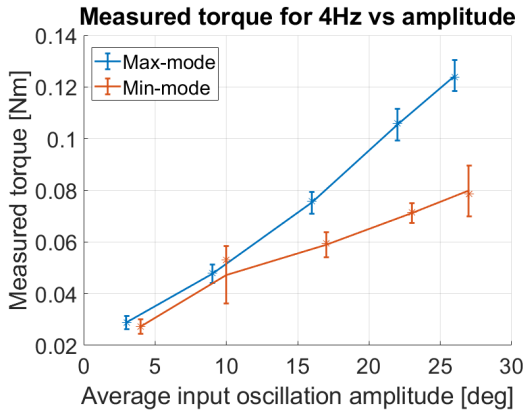

Figure 8: Errorbar plot of absolute peak torque of experiment one for both modes at 4 Hz. The Max-mode torque is substantially higher than that of the Min-mode, but only for amplitudes larger than 10 degrees. The asterisks ($*$) mark the medians, which are quite close to the mean, except for the Min-mode at 10 degrees. This may be an indication of a skewed distribution of the peak torque.

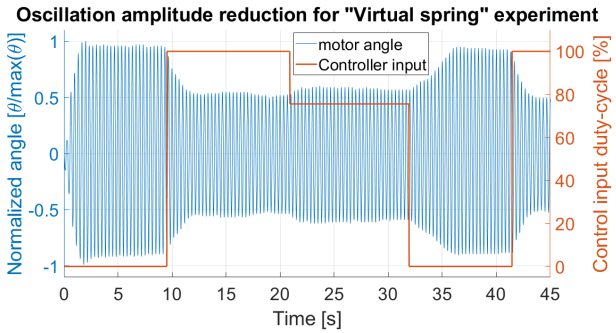

Figure 9: Motor angle over time with Virtual Spring-Controlled input perturbation of experiment two. The motor angle is normalized with respect to the maximum value in the dataset. The red line indicates the manually set duty-cycle shown on the right y-axis. Some lagging behavior is observed at the duty-cycle transition points

4.2 Damping torque variability

Figure 10 shows torque generated as a function of controller output provided by the third experiment. The distance between x-values depended on the observed torque difference from pilot experiments. As expected from Equation 13 the relation is inversely proportional. The theoretical estimate is calculated using only the electromagnetic part of the equation and a R_{switch} of $1 \times 10^5\,\Omega$.

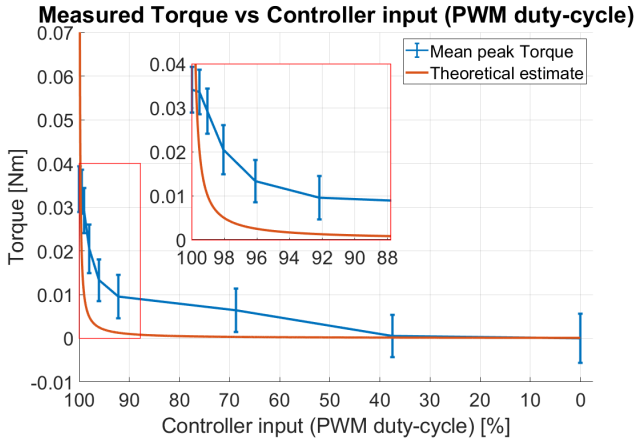

Figure 10: Errorbar plot of torque as a function of control input from experiment three data. The y-axis has been shifted such that the mean of the 0% duty-cycle trial corresponds to 0 N m. The theoretical data is calculated from Equation 13.

4.3 Frequency selective damping torque

The fourth experiment focused on the frequency selectivity of the prototype. Figure 11 shows the Power Spectral Density (PSD) of the measured torque for three experiment conditions. The condition with the prototype set to the input frequency shows the highest power at every frequency. The condition with the prototype set to 5 Hz shows near equal torque levels as the Min-mode for all frequencies, except at the chosen frequency of 5 Hz. Across the frequencies, both the baseline and the other conditions increase, while the difference between the Min-mode and the "set to input frequency"-condition is almost the same for all frequencies.

5 Discussion

5.1 Torque generation

Figure 7 shows that the prototype is able to generate an electromagnetic braking torque, but does not reach the target of 0.24 N m at any frequency-amplitude combination. Furthermore, the figure shows that below an amplitude of 10 degrees the mean peak torque difference is not consistently positive. This could be caused by mechanical hysteresis reducing the rotation time of the motor and also skewing the generated torque to one side of the oscillation.

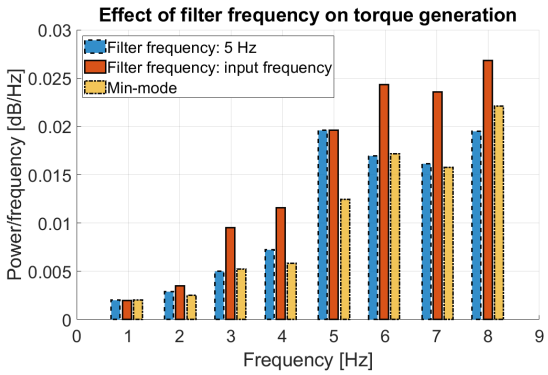

Figure 11: Frequency-dependent torque generation results from experiment four. Each bar shows the torque PSD for a separate trial, one for each frequency and condition. For the blue bars filter frequency is set to 5 Hz so the electromagnetic contribution to the measured torque should be highest at this frequency. By comparing the blue column with the yellow column it is seen that at 5 Hz the blue column is higher than the yellow. At all other frequencies the blue and yellow are closer together. The red columns show that if the filter setpoint frequency is equal to that of the input perturbation the torque PSD is consistently higher than the yellow columns (Min-mode).

Another explanation could be that the inertial torque of the motor is a bigger influence up to the 10 degree limit. This is illustrated by the absolute mean torque shown in Figure 8 for all amplitudes at 4 Hz. In this graph the data points between the Max-mode and Min-mode are actually shifted in the x-axis because actual measured mean motor amplitude is not the same for identical input signals. This is attributed to the platform controller not producing perfectly identical inputs for different conditions.

Despite the maximum torque difference not reaching the proposed requirements, the "virtual spring"-controlled experiments do show a suppression ratio of 50%. This suggests that the proposed required torque in Section 2 is an overestimation. A test setup or model capable of mimicking or simulating actual wrist dynamics will have to provide more substantial evidence for the prototype's closed-loop capabilities. The system also shows some lagging behavior upon changes in the duty-cycle up to 5 s. The slope of the peaks in the lagging sections looks strange compared to the expected exponential first-order responses to step inputs. This dynamic behavior is also not described in the current model and will need further investigation.

5.2 Torque variability

Figure 10 shows that there is a relation between the controller PWM value and the measured mean peak torque difference. This relation implies that the system is able to vary the damping-torque amplitude between the maximum and the minimum in an aproximately continuous way. The inverse proportional shape of the rela-

tion is as expected from Equation 9 and the resolution of the duty-cycle provides enough control over the damping torque in the steep region of the relation. The non-linearity of the relation could be better handled by more advanced control structures: Model predictive, Fuzzy control, Lookup-tables.

5.3 Frequency selective torque

The reason the damper has to be adaptive is traced back to the requirement that the device should reduce tremor with minimal effect on voluntary motion. It was hypothesized that variability of damper torque will allow for frequency-selective damping.

Experiment four shows that the prototype is able to autonomously detect a pre-set frequency and provide a damping torque to that frequency. Pilot experiments provided no conclusive evidence for the same behavior in the presence of multi frequency inputs. During the pilot experiments it was observed that the input amplitude only rarely exceeded the 10 degrees, which as seen from Figure 7 is below the electromagnetic effective threshold. A probable cause for this is the chosen signal type (Odd Multi-Sine) and the signal bandwidth. The bandwidth might have a too high with an upper bound of 12 Hz. The test-setup dynamics do not allow for the required high levels of acceleration and thus only rarely obtain the actual setpoint amplitude.

5.4 Prototype improvement

The proof of concept results show two areas where the current prototype is not meeting requirements. First the mean peak torque difference needs to be improved to meet the torque requirements. This also involves shifting the point of effect below 10 degrees as this is still a considerable wrist tremor, for which the prototype now only adds inertia without any adaptability. Secondly this involves the frequency selectivity of the generated damping. The prototype has only been tested in a single frequency environment, so more information is needed on multi-frequency input behavior. The prototype can be improved in both these aspects of with a couple of changes:

Motor choice The choice for the current electromotor could be improved by switching to a brushless dc-motor (BLDC). The comparison of motor back-EMF in Figure 12 between equally sized electromotors shows the BLDC with a higher back-EMF torque. Besides this, the BLDC has a steeper curve, but still a comparable friction torque curve compared to that of the DC motor. This means a large improvement in peak torque difference.

Gearbox ratio By increasing the gearbox ratio the motor velocity is increased for the same input velocity, however this also increases the inertial torque from the motor's rotor. It is hard to intuitively determine the effects, because the electrodynamic and inertial forces reach their maximum at a 90° phase difference. A parameter sensitivity analysis by partial derivation of Equation 10 to either K_t or N shows that the K_t value is much more dominant than N at maximum velocity. Although the K_t value has no effect at maximum acceleration for a pure sine input, the torque increase due to a change in gear ratio at maximum acceleration remains relatively small.
The problem with this comparison is that J_{rotor} and $J_{gearbox}$ are assumed to be constant for higher K_t and N values due to a lack of a relational model. Also the motor shaft damping and gearbox friction are not taken into account, which is a largely underestimated factor in the model.

Electromagnetic model The current prototype is setup with basic knowledge and a lot of simplifications to the electromagnetic interactions of the system. Torque amplitude is expected to improve if a specifically designed electromagnetic actuator is optimized using finite element modeling of the magnetics. Another uncertainty in the current model is the PWM switching between the open circuit and closed circuit states. This switching between system states is not accurately represented in the current formulas and thus the current understanding leaves out important factors that influence adaptability and stability of the damping torque.

Control strategy The choice for the control structure of the switches was kept simple, because the electromagnetic side of the model is not fully understood. Controller performance is expected to improve with the use of, for instance, model predic-

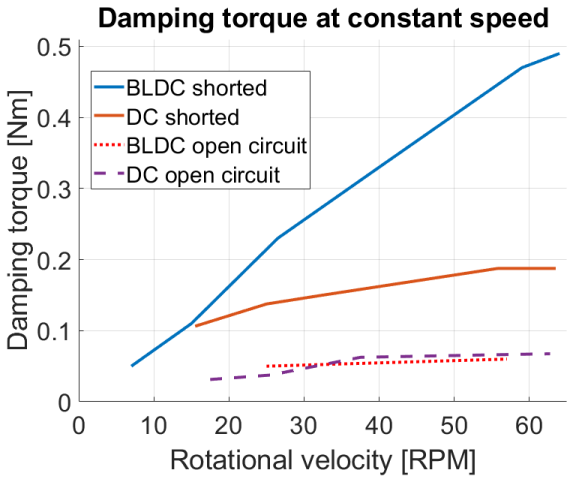

Figure 12: Comparison between max- and minimum back-EMF of BLDC and DC motor of comparable size. The x-axis is the motor rotor velocity and the y-axis is the measured torque from a torque sensor. The steepness of the BLDC torque curve shows that it generates more torque per RPM thus improving the peak torque difference with respect to the DC motor.

tive control. The addition of system knowledge to the control system enables it to react better to non-linear behavior.

Test setup A test setup capable of force controlled inputs for actual closed loop system operation testing provides better experiment fidelity. Closed loop tests are definitely needed to mimic the separation between voluntary and tremor forces, which is essential for validation of a concept before any trials on humans would be beneficial. Secondly, the current test setup was designed for multiple devices, so no approximation of wrist dynamics (J, B, K) was attempted. Either minimizing the test setup dynamics so more freedom of input perturbation is obtained, or tuning J, B, K to mimic human hand creates a setup capable of more informative input perturbations.

The results from this prototype validation provides a good basis for further development of a wrist tremor suppression device. With the gained knowledge of critical system components and their effects on system behavior a better prototype can be designed. Though not all validation targets have been reached the added knowledge gives STIL B.V. a foundation to continue development of the technology and work towards a functional wrist tremor orthosis.

6 | Conclusion

The objective of this thesis was to develop and evaluate an AEMD prototype capable of reducing tremor amplitude with minimal effect on voluntary motion. From the experimental results we can conclude that:

- The maximum torque generated by the prototype is only half of the validation target determined by the torque requirement of 0.24 N m. However, the second experiment shows that the obtained total torque differences are enough to reduce oscillation amplitude by 50% for a relatively large amplitude oscillation.

- The prototype is able to vary the electrodynamic damping torque given a constant input frequency. So the prototype passes the second validation target.

- No conclusive evidence for a higher SR than 13% has been obtained. Although, theoretically suppression of voluntary motion with perfect selectivity was two-thirds of the total, so the theoretical SR of this prototype would be 33% which is higher than the 13% from Loureiro et al.

Although optimization of system components and switch control still need to be investigated, the current results show the AEMD concept has promise for suppressing wrist tremor with less influence on voluntary motion than presented in recent research.

7 | Recommendations

If a more elaborate model is constructed with a better understanding of parameter dependances and scaling effects, the system can be parametrically optimized. This coupled with a more suited type of actuator (BLDC) and a test-setup capable of simulating the admissive character of a human wrist should enable future researchers to design a better second prototype capable of selective tremor suppression, which can compete with current treatment.

References

[1] Tremor in multiple sclerosis. *Journal of Neurology*, 254(2):133–145, 2007. doi: 10.1007/s00415-006-0296-7.

[2] M. Abbasi and A. Afsharfard. Modeling and experimental study of a hand tremor suppression system. *Mechanism and Machine Theory*, 126:189–200, aug 2018. doi: 10.1016/j.mechmachtheory.2018.04.009.

[3] J. Belda-Lois, E. Rocon, J. Sanchez-Lacuesta, A. Ruiz, and J. Pons. Estimation of biomechanical characteristics of tremorous movements based on gyroscopes. *Assistive Technologies: From Virtuality to Reality*, pages 138–142, 2005.

[4] A. P. L. Bó and P. Poignet. Tremor attenuation using FES-based joint stiffness control. *Proceedings - IEEE International Conference on Robotics and Automation*, pages 2928–2933, 2010. doi: 10.1109/ROBOT.2010.5509560.

[5] A. W. Buijink, M. F. Contarino, J. H. Koelman, J. D. Speelman, and A. F. van Rootselaar. How to tackle tremor - systematic review of the literature and diagnostic work-up. *Frontiers in Neurology*, OCT (October):1 – 12, 2012. doi: 10.3389/fneur.2012.00146.

[6] Central Intelligence Agency. The world factbook. URL `https://www.cia.gov/library/publications/the-world-factbook/fields/2010.html`. accessed: 2018-10-25.

[7] J. J. Chen and D. M. Swope. Essential tremor. *Journal of Pharmacy Practice*, 20(6):458–468, 2007. doi: 10.1177/0897190007311453.

[8] G. Deuschl, J. Raethjen, H. Hellriegel, and R. Elble. Treatment of patients with essential tremor. *The Lancet Neurology*, 10(2):148–161, 2011. doi: 10.1016/S1474-4422(10)70322-7.

[9] R. J. Elble. Diagnostic criteria for essential tremor and differential diagnosis. *Neurology*, 2000. doi: 10854344.

[10] R. J. Elble. *Neuro-Geriatrics*. Springer International Publishing, 2017. doi: 10.1007/978-3-319-56484-5.

[11] M. Elias, E. Maamary, L. Araneta, N. Obaid, and S. Patel. Apparatus for damping involuntary hand motions, 2018. WO2018053624A1.

[12] G. Grimaldi and M. Manto. *Mechanisms and Emerging Therapies in Tremor Disorders*. 2013. ISBN 9781461440260. doi: 10.1007/978-1-4614-4027-7.

[13] J. Kotovsky and M. J. Rosen. A wearable tremor-suppression orthosis. 35(4):373–387, 1998.

[14] C.-c. Liu, C.-y. Li, P.-c. Lee, and Y. Sun. Variations in incidence and prevalence of parkinson's disease in taiwan: A population-based nationwide study. *Parkinson's Disease*, pages 1–8, 2016. doi: 10.1155/2016/8756359.

[15] E. D. Louis and J. J. Ferreira. How common is the most common adult movement disorder? update on the worldwide prevalence of essential tremor. *Movement Disorders*, 25(5):534–541, 2010. doi: 10.1002/mds.22838.

[16] R. C. V. Loureiro, J. M. Belda-Lois, E. R. Lima, J. L. Pons, J. J. Sanchez-Lacuesta, and W. S. Harwin. Upper limb tremor suppression in ADL via an orthosis incorporating a controllable double viscous beam actuator. *Proceedings of the 2005 IEEE 9th International Conference on Rehabilitation Robotics*, 2005:119–122, 2005. doi: 10.1109/ICORR.2005.1501065.

[17] J. K. Monin, J. Gutierrez, S. Kellner, S. Morgan, K. Collins, B. Rohl, F. Migliore, S. Cosentino, E. Huey, and E. D. Louis. Psychological Suffering in Essential Tremor: A Study of Patients and Those Who Are Close to Them. *Tremor and other hyperkinetic movements (New York, N.Y.)*, 7:526, 2017. doi: 10.7916/D8Q53WF0.

[18] L. Popović Maneski, N. Jorgovanović, V. Ilić, S. Došen, T. Keller, M. B. Popović, and D. B. Popović. Electrical stimulation for the suppression of pathological tremor. *Medical & Biological Engineering & Computing*, 49(10):1187–1193, oct 2011. doi: 10.1007/s11517-011-0803-6.

[19] T. Pringsheim, N. Jette, A. Frolkis, and T. D. Steeves. The prevalence of parkinson's disease: A systematic review and meta-analysis. *Movement Disorders*, 29(13):1583–1590, 2014. doi: 10.1002/mds.25945.

[20] E. Rocon, J. M. Belda-Lois, A. F. Ruiz, M. Manto, J. C. Moreno, and J. L. Pons. Design and validation of a rehabilitation robotic exoskeleton for tremor assessment and suppression. *IEEE Transactions on Neural Systems and Rehabilitation Engineering*, 15(1):367–378, 2007. doi: 10.1109/TNSRE.2007.903917.

[21] T. D. Steeves, L. Day, J. Dykeman, N. Jette, and T. Pringsheim. The prevalence of primary dystonia: A systematic review and meta-analysis. *Movement Disorders*, 27(14):1789–1796, 2012. doi: 10.1002/mds.25244.

[22] E. J. Sternberg, R. N. Alcalay, O. A. Levy, and E. D. Louis. Postural and Intention Tremors: A Detailed Clinical Study of Essential Tremor vs. Parkinson's Disease. *Frontiers in Neurology*, 4(May):1–8, 2013. doi: 10.3389/fneur.2013.00051.

[23] J. Timmer, M. Lauk, S. Häußler, V. Radt, B. Köster, B. Hellwig, B. Guschlbauer, C. H. Lücking, M. Eicher, and G. Deuschl. Cross-Spectral Analysis Of Tremor Time Series. *International Journal of Bifurcation and Chaos*, 10(11):2595–2610, nov 2000. doi: 10.1142/S0218127400001663.

[24] P. Ylikotila, T. Tiirikka, J. S. Moilanen, H. Kääriäinen, R. Marttila, and K. Majamaa. Epidemiology of early-onset parkinson's disease in finland. *Parkinsonism and Related Disorders*, 21(8):938–942, 2015. doi: 10.1016/j.parkreldis.2015.06.003.

[25] A. H. Zamanian and E. Richer. Adaptive Disturbance Rejection Controller for Pathological Tremor Suppression With Permanent Magnet Linear Motor. In *Dynamic Systems and Control Conference, Volume 1*, number October, page V001T37A003. ASME, oct 2017. doi: 10.1115/DSCC2017-5151.

Appendices

A | Tremor suppression principle selection

A.1 Previous research

The concept currently under development at STIL B.V. is not applicable for wrist tremor suppression. To find a different operating principle a broad search into vibration suppression principles in various mechanical domains was conducted. A selection of principles was evaluated using a harris profile. The reported vibration suppression effects in other domains combined with results from recent research into mechanical tremor suppression methods provided a basis for selecting a new wrist tremor suppression principle.

A principle which is both effective in suppressing tremor without restricting the normal use of the wrist is desired. From Table 1 can be seen that this is accomplished by most active systems, however weight, size and power consumption complicates the fabrication of a fully wearable device. Previously researched passive concepts suppress at least two-thirds of voluntary motion or induce unwanted amplification. The research indicated as semi-active also reports high suppression of voluntary motion, but only one type of adaptable damper is evaluated. For the semi-active suppression category more principles were found in a literature study across mechanical fields.

Table 1: Tremor and voluntary motion suppression results from previous research for different types and principles. Some data was missing from the papers, so where possible estimates were made. For the pneumatic actuator of Taheri et al. no specs on the required compressor power could be found. Herrnstadt & Memon don't mention which motor is used for the suppression, so no estimate could be made. For both Zamanian & Richer and Rocon et al. a power estimate was made based on the motor's efficiency and the reduction in tremor power. Rocon et al. presented no suppression results on voluntary motion.

Author	Year	Category	Principle	Suppression		Weight	Power
				tremor	voluntary		
Hashemi et al.	2004	Passive	Tuned Mass Damper	80%	67%	130 g	0.0 W
Buki et al.	2018	Passive	Tuned Mass Damper	86%	-10%	280 g	0.0 W
Loureiro et al.	2005	Semi-Active	Magneto rheological damper	99%	86%	200 g	4.0 W
Case et al.	2013	Semi-Active	Magneto rheological damper	83%	96%	204 g	1.9 W
Taheri et al.	2014	Active	Pneumatic actuator	98%	<5%		
Herrnstadt and Menon	2016	Active	Rotational Electric motor	99%	0%	1,600 g	
Zamanian and Richer	2017	Active	Linear Electric motor	98%	<1%	265 g	4.0 W
Rocon et al.	2007	Active	Rotational Electric motor	82%		850 g	3.0 W

A.2 Harris Profile

A rubric (Table 2) is set up for systematic scoring of the different criteria in a Harris profile (Table 3). The different criteria are also multiplied with a factor indicating the relative importance between the different criteria. Each principle is then scored on each criterion with a value between -2 and 2, excluding 0.

Table 2: Rubric outlining the evaluation criteria used in the harris profile. The factors are determined in cooperation with the vision of STIL B.V

	Factor	Scope	+2	-2
Performance	3	Absolute tremor reduction potential.	>95% suppression for a wide range of tremor frequencies.	<60% suppression for a single predetermined frequency.
Safety	3	Potential for physical harm based on a criticality matrix.	Unlikely and minor health risks.	Occasional but severe health risks.
Compliance	3	Level of inhibition on voluntary movement.	Negligible suppression of frequencies below tremor frequency.	equal relative suppression across all frequencies
Range of motion	3	Possibility for reaching certain wrist postures without regard for required effort.	No change in range of motion.	Decrease to half of initial range of motion.
Ease of use	2	Required steps and effort for user.	Incidental maintenance and recharging after at least 12 hours.	Regular maintenance by the user and frequent charging of batteries.
Noise	2	Noise level during operation.	Occasional or silent, almost indistinguishable from background noise.	A frequent or continuous noise equal to speech volume.
Weight	2	Total mass needed for a working principle.	Addition of only $\frac{1}{4}$ times hand and arm mass.	Addition of weight equal to the mass of hand and underarm.
Size	2	Total system volume.	Equal or smaller than a tennis ball.	Bigger than a melon.
Cost	1	System cost based on availability and need for specialized suppliers.	Availability of stock parts with only small adjustments and a variety of suppliers.	Much need for specialized parts with limited suppliers.
Power	1	Expected electrical power use for control electronics.	Lower than estimated tremor power (1.4 W)	Twice as high as tremor power estimate.

The Harris profile is color-coded to create a more visually appealing way of representing the scores. The colorcoding also offers a quick way to identify the best and worst attributes for a given principle. The predominantly red and orange in the upper part of the passive principles section clearly shows the unsatisfactory performance of passive systems. The opposite is seen in the active principles, but these score badly in the criteria related to ergonomics and comfort. Thus a compromise with 'the best of both worlds' is found in de Semi-active concepts, with in particular AEMD scoring highest. This concept is essentially an electromotor with dynamic braking capability, which probably explains the close score between the active electromotor and semi-active AEMD.

Table 3: Color-coded Harris profile. Every criterion gets a score between -2 and $+2$ this is multiplied by the corresponding criterion weight and added in the bottom row for a total score.

		Principles											
		passive			semi-active						active		
		Viscous Damper	Damped Gyroscope	Electro-magnetic Damper	Electro Rheologi-cal damper	Magneto Rheo-logical Damper	Particle damper	Valve Damper	Adaptive Electro-magnetic Damper	Piezo- elec-tric Shunt Damper	Electric motor	Pneumatic motor	Active Gymbal Gyroscope
Criteria													
x3	Performance	-2	-1	-1	1	1	1	1	1	1	2	2	2
	Safety	2	1	2	-1	1	1	2	2	-1	1	-1	-1
	Compliance	-2	-2	-2	1	1	1	1	1	-1	2	2	2
	Range of motion	1	2	1	1	1	1	1	2	-1	2	2	2
x2	Ease of use	2	1	2	-1	1	1	1	1	1	1	-1	1
	Noise	2	-2	2	1	2	2	2	2	1	1	-2	-2
	Weight	-1	-1	1	-1	-1	-1	-1	1	2	-1	-1	1
	Size	-1	1	2	-1	-1	-1	-1	2	2	1	-1	1
x1	Cost	2	2	1	-1	-1	1	1	-1	-1	-1	-1	1
	Power	2	-1	2	-2	1	1	2	1	2	-1	1	-1
	Total Score	5	-1	17	-1	14	16	20	30	7	23	5	17

For more information on the principles compared in this Harris profile the reader is kindly referred to a literature study by the author. If this is not available to you it is possible to contact the author for a copy of the document.

B | Concept Synthesis

B.1 Morphological overview

The results of the Harris profile determine the Adaptable Electromagnetic Damper (AEMD) principle to be a promising basis for a wrist tremor suppression concept. The concept is based on the principle of electromagnetic braking, also called dynamic braking. Dynamic braking reverses an electromotor's working by turning kinetic energy of the motor's rotor into electrical energy, thereby damping the rotation. The rotor of the electromotor has permanent magnets that induce a current in the stator windings if the circuit is closed. This induced current creates an opposing magnetic field to that of the permanent magnets thereby providing a braking torque. This effect is called back-electromotive force (back-EMF).

The plan for this research was to construct a proof of concept and validate its performance in selectively suppressing tremor. A morphological chart in figure 13 has guided the choice of concept components and system structure. First the AEMD principle had to be divided into subfunctions. Possible physical implementations were proposed for all of the subfunctions. Next the physical implementations were combined into a number of plausible AEMD concepts. Finally these concepts were evaluated and a concept was chosen based on expected performance.

Options / Subfunctions	1	2	3	4	5	6
static magnetic field	Permanent magnet	Electromagnet				
Back-EMF Creation	Co-axial Rotation	Non-co axial rotation	Tangential Translation	Perpendicular translation	AC current	
Conductor shape	Disk	Plate	Coil	Cylinder	Square tube	
Measurement of wrist movement	Encoder	Intertial measurement	Hall effect	Laser	Strain gauge	Electromyography
Transmission of wrist movement	Gear	Belt	Leverarm	Hydraulics	Ballscrew	
Back-EMF Control / Throttle	gearratio	pulley diam	variable electric resistance	variable airgap	Magnetic field intensity	Electric reactive components

Figure 13: The table above is a morphological chart. The main function of the desired product is subdivided into subfunctions. The subfunctions each have multiple physical implementations. By combining subcomponents a concept can be created. Theoretically such a matrix has a lot of permutations, but by carefully selecting components which complemnent each other the nonsense concepts get filtered out in an early stage. On the other hand such a diagram helps the creative process by not ruling out individual implementations of subfunctions, because the value of a combination may be greater than that of the individual parts. The red green and blue dots denote three different concepts. If you follow one color from top to bottom, then you find the components for that concept.

Three concepts were identified with the most a priori expected potential from the morphological chart, indicated by the red, green and blue dots. These concepts were then evaluated for feasibility and tested with results from basic models and/or physical prototypes.

B.2 Linear Electromagentic Damper (Green)

The first concept (Green) is constructed from a permanent magnetic core, which translates inside a set of copper coils. A lever arm increases the stroke of the damper such that enough velocity can be built up. By connecting reactive electric components such as capacitors to the coil terminals the electric system can be tuned to allow current to flow for a specific set of frequencies.
The problem with this design was that due to the required length of the cylinder only part of the coils generated Back-EMF at any moment in time. The prototype also required a heavy steel magnetic core to direct the magnetic flux in the most effective way. This made the concept very volume and weight inefficient. Tests with a prototype linear electromagnetic damper supported that the volume-specific dampingforce was much less than required.

B.3 Back-driveable Ballscrew (Red)

The second concept (Red) uses a ballscrew to translate the linear translation of the dorsal side of the hand into a rotation around that direction. Unfortunately that linear translation turned out to be less than expected for an effective Back-EMF from an attached electromotor. Initially electrically filtering the back-EMF did seem to have a lot of potential, but that turned out to be impractical based on the required capacitance level(s) ($>$10 F). Besides this it also turned out that the torque required to backdrive the coilscrew would not be small compared to the required damping force. This meant that only a small amount of damping variation was possible, reducing the theoretical maximum selectivity of the damping force.

B.4 Adaptive Electromagnetic Damper (Blue)

The third concept (Blue) simplified the motion transmission by connecting a planetary gearbox in line with the wrist rotation axes. A dc-motor connected on the other side then generates a Back-EMF base on the wrist velocity scaled with the gear ratio. An added benefit was that most electromotors can easily be fitted with an encoder and thus the wrist angle and velocity were easily determined. The implementation of an electronically controlled variable resistance turned out more complex than was imagined during the concept development. The relatively high voltages and currents that would need to be regulated showed that a different approach was needed. To mimic the continuous behavior of an analog potentiometer it was proposed to use a transistor using a Pulse Width Modulated signal (PWM-signal). The electronic circuit would be loaded in two directions due to the reversal of motor Back-EMF polarity. Transistors often have a freeflowing direction, which would let current flow regardles of transistor state. That is why two transistors were needed to only allow current to flow from motor to ground trough one transistor at a time. The two transistors and their relative connection is seen in Figure 4.

C | Separation of tremor from voluntary movement

The Normalized Peak Filter (NPF) described in this research is used to separate tremor frequencies from voluntary movement frequencies. The advantage of the NPF over high-pass filtering or other frequency identification techniques is that this filter induces no phase delay at its center frequency. Figure 14 shows the bode diagram of the filter with a center frequency set to 3 Hz. Besides the frequency also the bandwidth and sample frequency have to

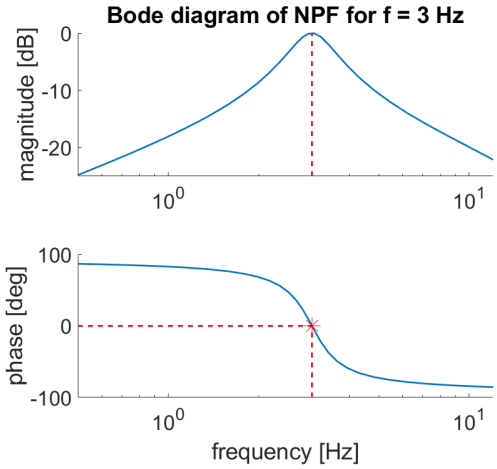

Figure 14: Bode diagram of the NPF. It can be seen that the set center frequency of three hertz has the maximum gain and no phase shift. The steepness of the peak can be adjusted by a bandwidth parameter, but this also affects the filter's settling time.

be set. The bandwidth determines the sharpness of the peak, but it also results in some lead-in behavior of the filter visible in Figure 15. If the center frequency of the filter is coincident with the tremor frequency then the output is the undistorted tremor signal with almost no voluntary movement components. For this study all experiments were designed with constant frequency content so it sufficed to set the filter frequency before each trial. For actually filtering a tremor signal it is necessary to determine the tremor frequency and shift the filter center frequency accordingly.

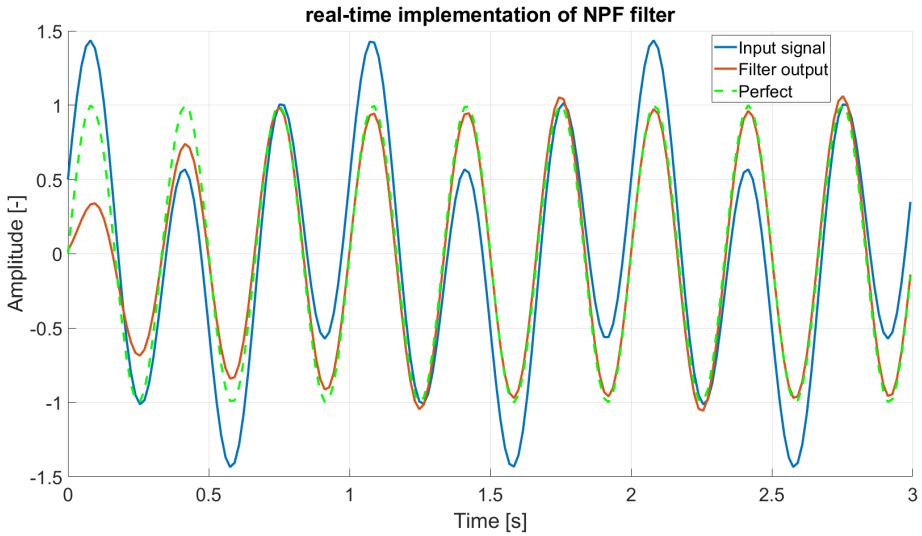

Figure 15: A signal with two sinusoids super imposed is filtered by the NPF. The low frequency oscillation of 1 Hz is almost completely absent after filtering.